Hindawi Publishing Corporation
ISRN Corrosion
Volume 2013, Article ID 424805, 8 pages
http://dx.doi.org/10.1155/2013/424805

Research Article

One-Step Anodization/Sol-Gel Deposition of Ce^{3+}-Doped Silica-Zirconia Self-Healing Coating on Aluminum

N. Kumar, A. Jyothirmayi, K. R. C. Soma Raju, V. Uma, and R. Subasri

International Advanced Research Centre for Powder Metallurgy and New Materials (ARCI), Balapur, Hyderabad, Andhra Pradesh 500005, India

Correspondence should be addressed to R. Subasri; subasri@arci.res.in

Received 5 September 2013; Accepted 8 October 2013

Academic Editors: M. Aparicio, G. Bereket, and M. Sakairi

A novel process was used for the preparation of dense, thick, and stable silica-zirconia coatings on aluminum by an *in situ* anodization along with sol-gel deposition. Anodic electrophoretic deposition was carried on aluminum using a SiO_2-ZrO_2 sol that was synthesized from an epoxy modified silane and zirconium n-propoxide along with a cerium salt ($Ce(NO_3)_3{\cdot}6H_2O$). Current density and time were varied during the deposition. The optimal parameters that yielded uniform coatings were determined. Coatings were characterized for their crystallinity, scratch hardness, and microstructure. The barrier properties of the coatings were tested using potentiodynamic polarization studies, electrochemical impedance spectroscopy, and neutral salt spray tests. Grazing angle incidence X-ray diffraction studies revealed that the coating comprised crystalline Al_2SiO_5 along with an amorphous phase. The novelty of the process was that the crystalline aluminosilicate phase was formed even at room temperature and could be deposited on aluminum by a simultaneous anodization of aluminum and sol-gel deposition. The coated substrates withstood more than 400 hours of salt spray tests. Polarization measurements reveal that the composite layer of aluminosilicate along with the Ce^{3+}-doped silica-zirconia sol enhances the corrosion properties by forming a passive layer, which acts as a good barrier against corrosion.

1. Introduction

Aluminum, that is widely used as a structural material due to its high strength to weight ratio and low cost, is highly susceptible to corrosion attack in chloride containing environment [1, 2]. Chromate conversion coatings have been the most widely used self-healing, anticorrosion treatments for aluminum and its alloys. Due to the increasing demand for the development of an environmentally-friendly, effective, inexpensive, and technologically simple method for corrosion protection, anodization of aluminum, and conversion coatings based on vanadates, permanganates, tungstates, and rare-earth salts have recently attracted a lot of attention as a method for corrosion protection [3]. Anodization is an electrochemical oxidation process employed to increase the thickness of the native oxide layer on metals like Al, Mg, Ti, and so forth [4–15]. The anodized layer is porous and, hence, there are reports in which a sol-gel coating is deposited on top of the anodized layer to render good barrier properties [16, 17]. There are also reports where, initially, a purely inorganic sol-gel coating is deposited on the aluminum substrate, followed by heat treatment at high temperatures (300–500°C) for densification, and then the substrate is subsequently anodized [18, 19] in an effort to obtain the cumulative benefits of both processes, namely, anodization and sol-gel coating. However, a low processing temperature for coating densification is one of the most important requisites, since some metals like aluminum undergo structural changes with temperature which degrade the mechanical properties of the substrate and promote corrosion [20]. The sol-gel organic-inorganic hybrid coating is a promising alternative that offers several advantages such as low temperature densification, good adhesion with the substrate, cost-effectiveness, being eco-friendly, and simple application procedures, which are

easily adaptable by the user-industry. The sol-gel hybrid matrices can also be used for encapsulating self-healing materials [21, 22].

The present work describes a novel process where aluminum substrate is dipped in a silica-zirconia hybrid sol containing Ce^{3+} which acts as a self-healing material and anodic electrodeposition is carried out. Under these conditions, aluminum can be simultaneously anodized forming, *in situ*, a crystalline aluminosilicate layer on the substrate surface, along with the deposition of sol-gel coating on the crystalline aluminosilicate layer. The pH of the sol, current density, deposition time, and curing temperature were optimized to form a defect-free, dense, and corrosion resistant oxide layer.

2. Experimental

2.1. Materials and Synthesis. 3-Glycidoxypropyltrimethoxysilane (GPTMS, Gelest Inc., USA, purity > 97%), zirconium n-propoxide (GELEST Inc., USA), methacrylic acid (ABCR GmbH, Germany, purity > 97%), and high purity solvent 2-butoxyethanol (LR grade) (Sd Fine-Chem. Ltd., India) were used as the starting materials without further purification. Cerium nitrate ($Ce(NO_3)_3{\cdot}6H_2O$) 99.9% (LOBA CHEMIE Pvt., India) was used as the source of Ce^{3+}. Aluminum specimens, obtained from Q-Lab Florida, USA, with dimensions 40 mm × 30 mm × 1 mm, were used as anodes after thorough degreasing with acetone. The chemical composition of the aluminum substrate in wt% was Al-98; Mn-1; Si-0.6; Zn-0.1; Cu-0.05–0.3. The sol was synthesized in two parts and then mixed together to obtain the nanocomposite sol. In the first step, zirconium-n-propoxide was complexed with methacrylic acid in a mole ratio of 1 : 1 under vigorous stirring to reduce the hydrolysis rate of Zr-n-propoxide. In the second step, GPTMS and water mixture was stirred with 0.1 N HCl for prehydrolysis of GPTMS and after ensuring hydrolysis of GPTMS, both parts were mixed and stirred continuously for 5 h. The mole ratio of GPTMS : Zr-n-propoxide was 3 : 1. The sol (henceforth abbreviated as GZ) was then appropriately diluted using 2-butoxy-ethanol and cerium nitrate was added so that final concentration of Ce^{3+} in the sol was 0.01 M.

2.2. Anodization/Deposition. The coating was deposited electrochemically using the inorganic-organic hybrid sol (GZ sol), along with Ce^{3+} as the source of self-healing material. A programmable current source (Keithley 224) was used for supplying the current during the deposition process. The process of anodization/deposition was monitored with current source as well as withdrawal speed. The pH of the sol was varied in three steps, namely, 4, 8, and 10. The current density was varied between 1.2 and 4 mA/cm^2 in three steps, namely, 1.2 mA/cm^2, 2.4 mA/cm^2, and 4 mA/cm^2, and the time of immersion of substrates in the sol was also varied for 1, 5, and 10 minutes. The optimum conditions were found to be the deposition of a sol maintained at pH 8–8.5 using a current density 4 mA/cm^2 for a deposition time of 10 minutes. After the layer formation on the substrate, it was removed from the sol tank using a dip coater with 1 mm/s withdrawal speed. The coatings were cured in air at 130°C for 1 h. Some of the coatings were also cured in air at 300°C for 1 h. For the sake of comparison, normal dip coating of the sol was also carried out on some of the substrates using 1 mm/s withdrawal speed and coatings were cured at 130°C for 1 h.

2.3. Characterization. The coating thickness, morphology, and composition were analyzed by SEM/EDAX, using a scanning electron microscope (Hitachi model S/3400N) and the crystalline nature was ascertained using an X-ray diffractometer (Bruker D8 AXS Advance X-ray diffractometer), using both normal incidence (NI) and grazing angle incidence (GI) of 1 degree. The adhesion of the coatings was tested according to ASTM D3359-02. Scratch test is a simple and rapid method to characterize the coatings, but results obtained are influenced by various factors such as coating thickness, mechanical properties of the substrate, interfacial bond strength, and test conditions such as scratch speed, load, and indenter tip radius. Scratch test was carried out using a microscratch tester (Revtest, CSM make). A Rockwell diamond indenter with a tip radius of 200 μm and a progressive loading method from a minimum of 0.9 N at the point of contact to a maximum of 10 N normal load at the end of scratch length were employed for evaluating the coated substrates. Scratch length, loading rate, and scratching speed were fixed at 6 mm, 7.58 N/min, and 5 mm/min, respectively. In the present investigation, the scratch tester tip was brought in contact with the coated surface and the sample was moved at a constant speed, while the tip normal load was progressively increased to the set maximum value. The output was measured in terms of acoustic emission, penetration depth, and tangential frictional force. The scratch tester has a tip, which is placed with a controlled scratch load F_z on the surface to be tested. When the sample is scratched, the tip is stationary and sample moves. The resulting frictional force F_x can be monitored, while the scratch track is generated.

Electrochemical tests were carried out using an electrochemical interface (Solartron SI 1287) with an impedance analyzer (Solartron SI 1260). The corrosion test cell had the classic configuration of three electrodes, platinum electrode as counter electrode, a saturated calomel electrode as a reference electrode, and the uncoated/coated aluminum substrate as the working electrode. Polarization studies of the coated/uncoated substrates were carried out at 25°C in a N_2 purged 3.5% NaCl solution with an exposure time of 1 h and 24 h. Potentiodynamic scans were recorded by applying potentials from −1.6 V to 0.0 V with a scan rate of 1 mV/s. The electrochemical impedance scan was carried out using an AC signal of 10 mV amplitude applied over a bandwidth from 100 kHz to 0.03 Hz. The corrosion behavior was also tested by neutral salt spray tests, using 5% NaCl solution according to ASTM B117.

3. Results and Discussion

3.1. XRD Analysis. Structural properties were investigated with both normal incidence XRD and GIXRD, the latter being a surface sensitive technique. The grazing incidence method was employed due to the large penetration depth of

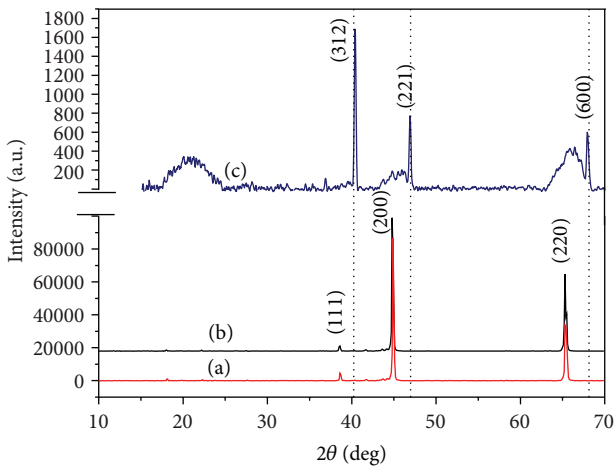

Figure 1: Comparison of XRD patterns of (a) bare aluminum, (b) coated aluminum cured at 130°C, both acquired at normal incidence and (c) that of coated aluminum, cured at 130°C, acquired at GI of 1 degree.

X-rays into the bulk during normal incidence, which tend to add diffraction peaks from the underlying crystalline matrix of the substrate to that of the coating on the surface, thereby masking the information due to the coating. Figure 1 presents the comparison of the normal incidence XRD patterns of bare aluminum (Figure 1(a)) and that of the coated aluminum (Figure 1(b)), which was cured at 130°C. However, it can be clearly seen that both patterns look similar. Due to high penetration depth of X-rays, the information from the coating has been masked due to the highly crystalline nature of the metallic substrate. Figure 1(c) shows the XRD pattern obtained from the GIXRD analysis. Here, it can be clearly seen that there is an initial hump, which is an indication of presence of an amorphous phase along with sharp peaks that indicate presence of a crystalline material. Since the peaks do not coincide with those of the aluminum substrate (JCPDS 04-0787), it can be inferred that these peaks are due to a different phase in the coating, which correspond to an aluminosilicate with the formula Al_2SiO_5 (JCPDS 44-0027). The XRD analysis shows that the formed material during the *in situ* anodization/sol-gel deposition process is crystalline on an as-deposited sample, even at room temperature. The amorphous phase in the coating could be silica and/or zirconia from the GZ sol.

3.2. SEM/EDAX Analysis. An image of cross section of the coated aluminum substrate is shown in Figure 2(a). The coating is seen to be 15–20 microns thick and the EDAX spectrum of the coating is shown in Figure 2(b). It can be seen from Figure 2(a) that the coating is highly dense in nature. The SEM images of the surface of the coated sample as shown in Figure 3 confirm that the coating is dense with negligible surface porosity. The coatings cured at 130°C (as shown in Figure 3(a)) do not show any defects. However, when the coatings are heat-treated at 300°C, the magnified image of the surface (inset shown in Figure 3(b)) confirms that cracks had

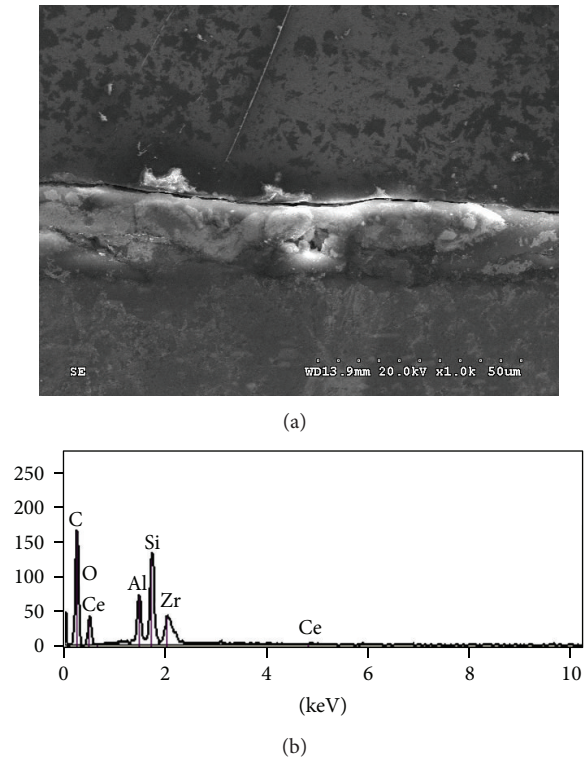

Figure 2: (a) SEM image of cross section of coated Al. (b) EDAX spectrum of the indicated area of (a).

appeared in the coating. Hence, it was concluded that a low temperature of 130°C for curing was sufficient to remove the residual solvent, densify, and generate a defect-free coating.

3.3. Scratch and Adhesion Test. The onset load for coating cracking is commonly referred to as the critical load and is associated with the rise in values of coefficient of friction and acoustic emission. In the present case, the frictional load and the acoustic emission were not clearly distinguishable as the coatings started to crack at about 2 N normal loads. Hence, morphology of the scratch was considered to rank the coatings for simple dip coated and electrolytically deposited coatings that were abbreviated as SD and ED, respectively.

From the scratch test results, the simple dip coated specimen started showing visible cracks and delamination even at the bare minimum load of 0.9 N applied during point of contact, whereas there were no cracks in the electrolytically coated specimens till the normal load increased to 2 N. The loads mentioned here are the average values of three scratch tests carried on each sample at different locations. These are the critical loads for the respective coating conditions. Normally, small fractures are generated across the scratch length with increasing load at certain periodicity. However, the coatings still stay adhered to the substrate till a second critical load. But when the normal load rises further, coating delaminates forming debris on the sides of the scratch. Scratch tracks are visible even to the naked eye due to the scattering of light by the defects along the width and/or depth of the scratch. While the SD sample has failed in

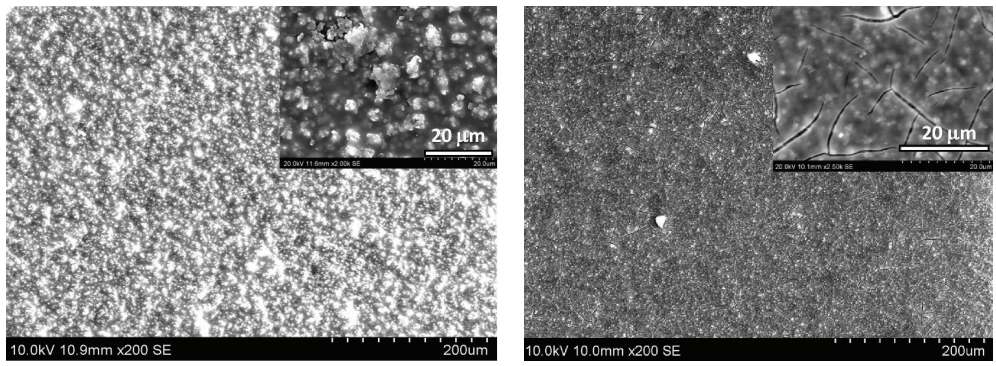

(a) (b)

Figure 3: SEM images of the surface of coated substrate (a) cured at 130°C and (b) cured at 300°C.

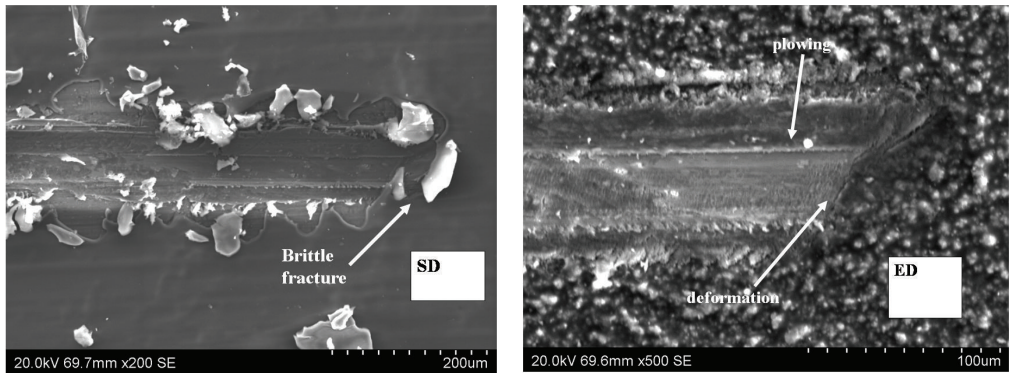

(a) (b)

Figure 4: SEM images of scratch (a) simple dip coated (SD) and (b) electrolytically deposited (ED) aluminum.

classic brittle fracture as can be discerned from Figure 4(a), ED failed according to classic ductile fracture as seen in Figure 4(b). The results from the scratch tests can be further understood by examining the morphology of the ED samples by SEM analysis. The coatings have a microlevel roughness with extensive porosity due to dendrite-like structure as seen from the inset of Figure 3(a). But these dendrites and the pores are covered with a layer of the silica-zirconia formed from the sol. These dendrites have further submicron and nanoparticle structure resulting from the ED process. Such structure acts like a reinforcement and provides necessary improved tensile strength. Hence, the ED coatings are able to resist the brittle fracture at lower load unlike a normal sol-gel coating, though the coating material is the same. Accordingly, the dendrite structure in case of the former is rougher due to enhanced height of such features. The adhesive properties were tested for ED coatings and were found as 5B (0% removal after adhesion test), which implies that the coating has excellent adhesion to the substrate.

3.4. Corrosion Tests

3.4.1. Neutral Salt Spray Tests (NSST). The photographs of coated and bare substrates after NSST are shown in Figure 5. The substrate panels were scratched prior to exposure to salt spray to accelerate the corrosion process. The bare aluminum panel totally failed in 48 hours, while the coating in the normal dip coated substrate started to peel off after 48 hours and the scratched area was filled with the corrosion product. In case of electrochemically anodized cum deposited substrate (ED), no corrosion was found to occur even after 400 hours. The performance of the ED coating as a barrier coating is far superior to simple dip coated aluminum and is capable of rendering a long-term corrosion protection to the aluminum substrate and, hence, further corrosion resistance property measurements like potentiodynamic polarization and electrochemical impedance studies were carried out only on ED samples and not on the SD samples.

3.4.2. Potentiodynamic Polarization Measurements. The data obtained from the potentiodynamic polarization studies carried out after 1 h and 24 h exposure to 3.5% NaCl, on the electrolytically coated aluminum and bare aluminum substrates are presented in Figure 6 and the results obtained after R_p fitting the data are presented in Table 1. It could be seen that the electrolytically coated Al provided a good barrier protection to the aluminum substrate, since the corrosion current density, i_{corr}, was lower when compared to that for the bare aluminum substrate. The corrosion potentials were lower for the coated aluminum substrates when compared to

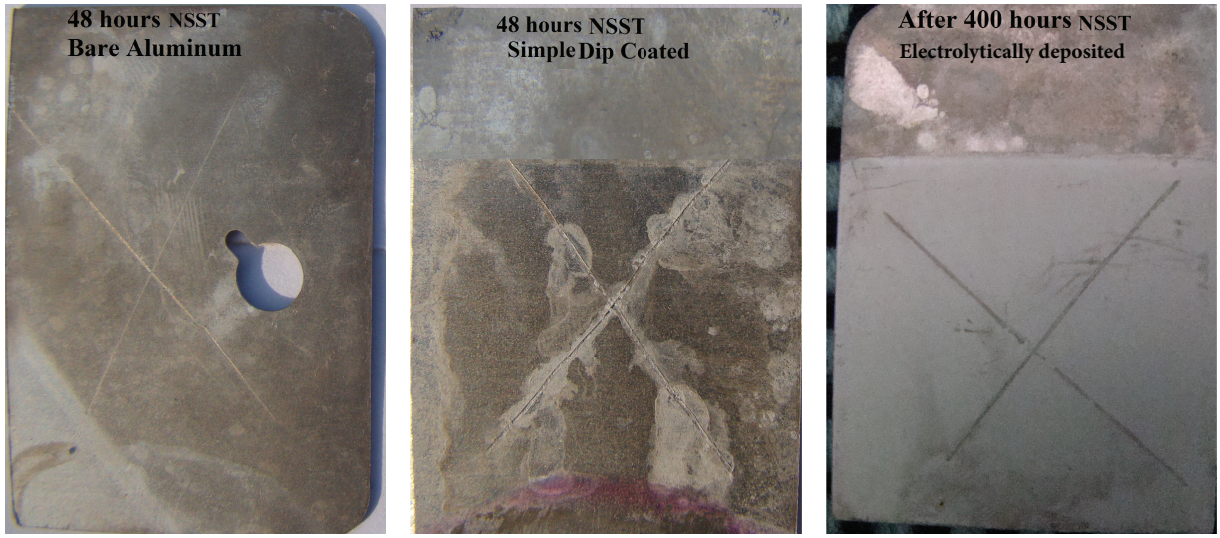

Figure 5: Photographs of samples after salt spray test: (a) after 48 hours—bare aluminum substrate, (b) after 48 hours—dip coated substrate with 3 mm/s withdrawal speed, and (c) after 400 hours—electrolytically deposited substrate.

Table 1: R_p fit data for the results obtained from potentiodynamic polarization measurements.

Sample	E_{corr} (Volts)	I_{corr} (Amp/cm^2) $\times 10^{-7}$	R_p (Ohms/cm^2)
Bare Al-1 h	−0.806	64.104	4069.4
Bare Al-24 h	−1.059	15.849	16460
ED-1 h	−1.409	5.247	49714
ED-24 h	−1.377	2.513	1.038*E*5

those for the bare Al substrate. The reduction in the open circuit potential (OCP) could be attributed to the effective suppression of the cathodic reaction due to the reason that SiO_2 having a low isoelectric point (IEP = 1.7 − 3.5) leads to a negative surface charge at pH > 2. Since the coatings are exposed to the electrolyte solution 3.5% NaCl that has a pH from 6.5 to 7, which is higher than the IEP, the open circuit potential of the coated substrate is more negative than that of the bare substrate. Though the coatings had lower corrosion potentials than bare Al, they provided a good barrier effect and reduced the corrosion currents.

In case of only the bare Al, after 1 h exposure, the i_{corr} value is higher in magnitude when compared to that of the 24 h exposure, which implies the formation of an oxide layer during longer exposure time. The oxide layer formation is evident by the passive region formation from −1.0 V to −0.70 V (300 mV), which decreases the rate of corrosion during longer periods of exposure to the electrolyte solution as shown in Figure 6.

It has been reported that the presence of Ce^{3+} in an electrolyte solution reduces the rate of oxygen reduction reaction and E_{corr} shifts to more negative values when compared to that without Ce^{3+} ions [23, 24]. In the present case, the Ce^{3+} ions were present in coating itself. In case of the coated substrates exposed to the electrolyte solution for 1 and 24 h,

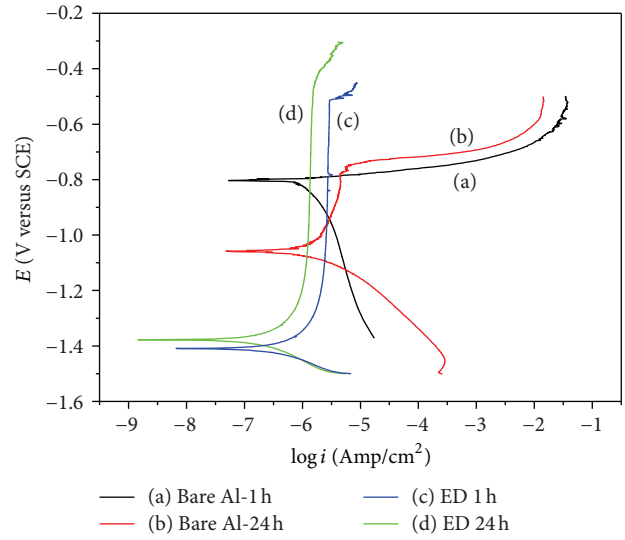

Figure 6: Potentiodynamic polarization plots of bare and coated Al (with ED) after 1 h and 24 h exposure to 3.5% NaCl solution.

namely, ED-1 h and ED-24 h, the cathodic arm was shifted to more negative potentials and also lower current densities, when compared to the bare aluminum substrate, indicating a reduction in the rate of oxygen reduction reaction as shown in Figure 6. The corrosion resistance is much higher for the ED samples when compared to that for bare Al for both exposure times. A well-established passive region can be observed for ED samples for 1 h exposure itself and it is still improved for 24 h exposure. This shows that the coatings are highly protective. The 900 mV, that is, the difference between E_{corr} (corrosion potential) and E_c (breakdown potential), is associated with the increased corrosion resistance of passive coatings as shown in Figure 6.

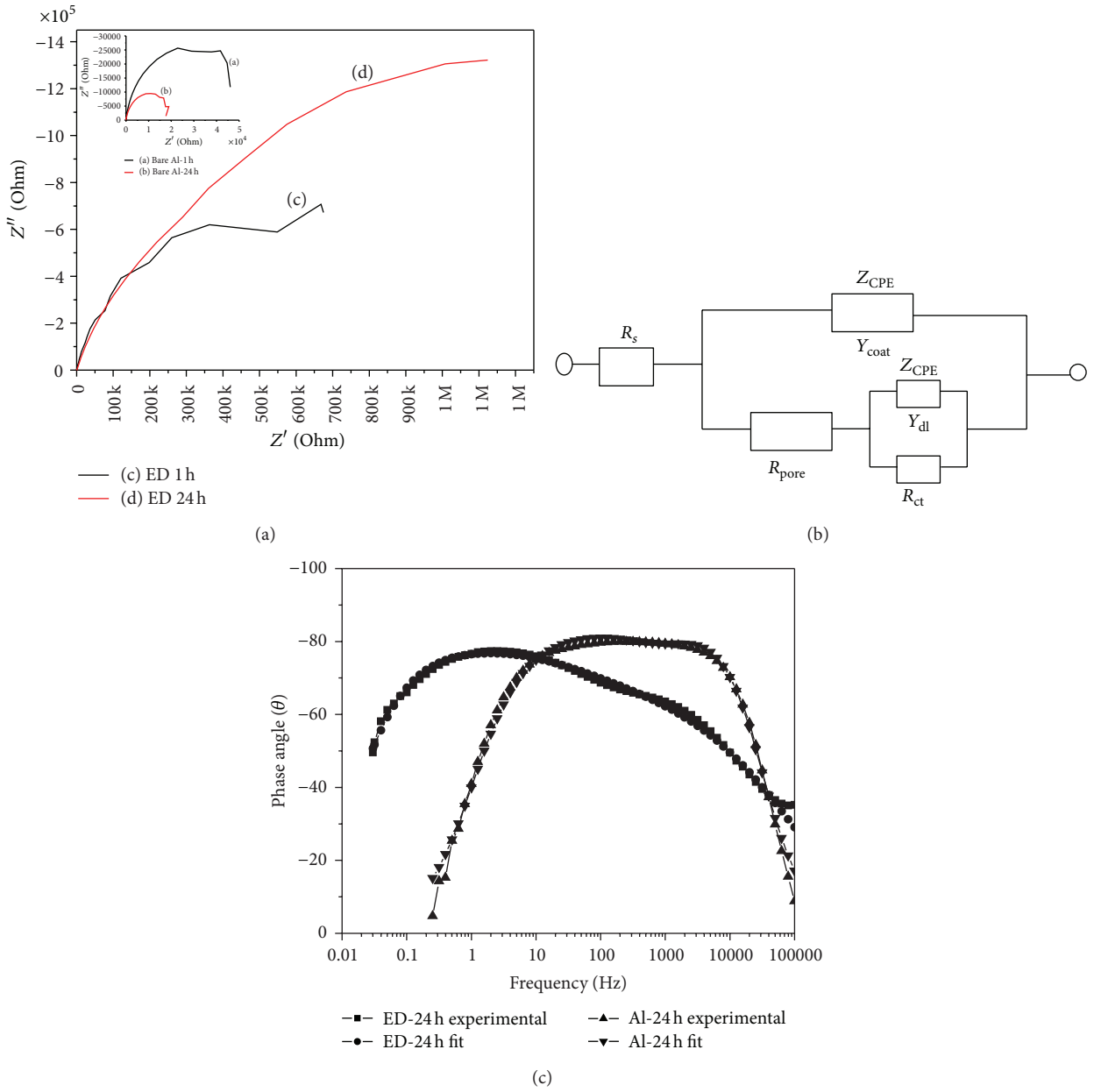

FIGURE 7: (a) Nyquist plots for the coated and bare Al for 1 h and 24 h exposure to 3.5% NaCl, (b) equivalent circuit used for fitting the EIS data of coated substrate, and (c) Bode plot for bare aluminum and ED coating on aluminum after 24 h exposure to 3.5% NaCl.

3.4.3. Electrochemical Impedance Spectroscopy (EIS). EIS is a nondestructive testing technique for evaluation of the barrier properties of the coatings and adhesion to the substrate. The obtained EIS data for the coated substrates are shown as Nyquist plots in Figure 7(a) and were fitted using the equivalent circuit given by two time constants as shown in Figures 7(b) and 7(c).

A constant phase element (CPE) was used instead of an "ideal capacitor" to explain the deviations from ideal behavior. The possible reasons for a nonideal behavior could be due to surface roughness, inhomogeneous reaction rates on the surface, varying thickness, or composition of a coating [25–27]. The time constant at high frequencies is related to the properties of coating and that at medium and lower frequencies is related to the properties of substrate. The impedance of a CPE, that is, Z_{CPE}, could be defined as $Z_{CPE} = 1/Y(j\omega)^n$, where ω is the angular frequency in rad·s^{-1}, Y is the pseudocapacitance, and n is called the CPE exponent, which is associated with the system inhomogeneity. When $n = 1$, the system behaves like a pure capacitor and $Y = C$. When CPE is used to fit the experimental data, $n < 1$; R_s is the resistance of the electrolyte; R_{pore} is the resistance to charge transfer through pores; Y_{coat} is the pseudo-capacitance of coating; Y_{dl} is pseudocapacitance associated with the double layer formed at the metal-electrolyte interface in parallel with charge transfer resistance R_{ct} describing the corrosion of the

Table 2: Results after fitting the EIS data for the bare and ED aluminum substrates after 1 h and 24 h exposure to 3.5% NaCl.

Sample	R_s ($\Omega\cdot cm^2$)	Y_{coat} ($Ss^n cm^{-2}$)	n	R_{pore} ($\Omega\cdot cm^2$)	Y_{dl} ($Ss^n cm^{-2}$)	n	Rct ($\Omega\cdot cm^2$)	χ^2
Bare Al-1 h	2.37	$7.88E-7$	0.97	70.44	$4.76E-6$	0.83	$6.04E4$	0.003
Bare Al-24 h	1.54	$3.38E-6$	0.96	124.7	$5.89E-6$	0.81	$2.11E4$	0.011
ED-Al-1 h	27.47	$5.56E-7$	0.79	163.5	$3.20E-6$	0.91	$2.02E6$	0.015
ED-Al-24 h	27.34	$1.26E-6$	0.83	637.2	$8.07E-7$	0.86	$4.34E6$	0.011

metal substrate. Table 2 presents the EIS results after circuit fitting of bare and ED samples exposed to 3.5% NaCl for 1 h and 24 h. It can be seen from Figure 7(a) and Table 2 that the R_{ct} values of the ED samples are higher by two orders of magnitude than those of bare samples after 1 h and 24 h exposure which shows that the coating does not allow the electrolyte to penetrate and reach the substrate. Even the R_{pore} values were also found to be higher (refer to Table 2) for coated samples at both exposed timings than those for bare Al substrate, showing less porosity in the coatings. The higher R_{pore} value of ED sample exposed for 24 h is due to closing of the existing pores by Ce^{3+} ions which are converted into $Ce(OH)_3$ and $Ce(OH)_4$ precipitates.

4. Conclusion

The novel process of *in situ* anodizing/sol-gel coating deposition substantially improved the corrosion resistance properties of the aluminum substrate and as expected, this one-step anodizing/deposition process circumvents the deterioration of mechanical properties of substrate due to the process being carried out at room temperature process which does not need high temperature curing. The SEM studies suggest that a low temperature of 130°C is sufficient for curing to obtain crack-free coatings. Since this coating is highly stable in salt spray test, it has considerable potential as future alternatives for nontoxic chromate-free conversion coatings.

Acknowledgments

The authors gratefully acknowledge the constant support and encouragement provided by Dr. G. Sundararajan and Dr. G. Padmanabham, ARCI, Hyderabad, India. The authors also would like to acknowledge Mr. G. V. R. Reddy for the SEM analysis and Mr. A. Ramesh for the technical support.

References

[1] M. P. Ryan, D. E. Williams, R. J. Chater, B. M. Hutton, and D. S. McPhail, "Why stainless steel corrodes," *Nature*, vol. 415, no. 6873, pp. 770–774, 2002.

[2] I. Betova, M. Bojinov, T. Laitinen, K. Mäkelä, P. Pohjanne, and T. Saario, "The transpassive dissolution mechanism of highly alloyed stainless steels: I. Experimental results and modelling procedure," *Corrosion Science*, vol. 44, no. 12, pp. 2675–2697, 2002.

[3] S. A. Kulinich and A. S. Akhtar, "On conversion coating treatments to replace chromating for Al alloys: recent developments and possible future directions," *Russian Journal of Non-Ferrous Metals*, vol. 53, no. 2, pp. 176–203, 2012.

[4] V. Moutarlier, M. P. Gigandet, and J. Pagetti, "Characterisation of pitting corrosion in sealed anodic films formed in sulphuric, sulphuric/molybdate and chromic media," *Applied Surface Science*, vol. 206, no. 1–4, pp. 237–249, 2003.

[5] S. J. Garcia-Vergara, P. Skeldon, G. E. Thompson, and H. Habazaki, "A tracer investigation of chromic acid anodizing of aluminium," *Surface and Interface Analysis*, vol. 39, no. 11, pp. 860–864, 2007.

[6] L. E. Fratila-Apachitei, F. D. Tichelaar, G. E. Thompson et al., "A transmission electron microscopy study of hard anodic oxide layers on AlSi(Cu) alloys," *Electrochimica Acta*, vol. 49, no. 19, pp. 3169–3177, 2004.

[7] X. Liu, J. Gen, A. Yu, G. Wang, L. Song, and X. Zhang, "A study on a submerged membrane bioreactor for municipal wastewater treatment," *Advanced Materials Research*, vol. 531, pp. 415–418, 2012.

[8] A. Jagminas, D. Bigeliend, I. Mikulskas, and R. Tomasiunas, "Growth peculiarities of aluminum anodic oxide at high voltages in diluted phosphoric acid," *Journal of Crystal Growth*, vol. 233, no. 3, pp. 591–598, 2001.

[9] R. Narayanan and S. K. Seshadri, "Phosphoric acid anodization of Ti–6Al–4V—structural and corrosion aspects," *Corrosion Science*, vol. 49, no. 2, pp. 542–558, 2007.

[10] S. J. Garcia-Vergara, P. Skeldon, G. E. Thompson, and H. Habazaki, "Pore development during anodizing of Al-3.5 at.%W alloy in phosphoric acid," *Surface and Coatings Technology*, vol. 201, no. 24, pp. 9506–9511, 2007.

[11] F. L. Coz, L. Arurault, S. Fontorbes, V. Vilar, L. Datas, and P. Winterton, "Chemical composition and structural changes of porous templates obtained by anodising aluminium in phosphoric acid electrolyte," *Surface and Interface Analysis*, vol. 42, no. 4, pp. 227–233, 2010.

[12] M. A. Song-jiang, L. Peng, Z. Hai-hui, F. U. Chao-Peng, and K. Ya-fei, "Preparation of anodic films on 2024 aluminum alloy in boric acid-containing mixed electrolyte," *Transactions of Nonferrous Metals Society of China*, vol. 18, no. 4, pp. 825–830, 2008.

[13] H.-H. Shih and S.-L. Tzou, "Study of anodic oxidation of aluminum in mixed acid using a pulsed current," *Surface and Coatings Technology*, vol. 124, no. 2-3, pp. 278–285, 2000.

[14] M. A. Páez, J. H. Zagal, O. Bustos, M. J. Aguirre, P. Skeldon, and G. E. Thompson, "Effect of benzotriazole on the efficiency of anodizing of Al-Cu alloys," *Electrochimica Acta*, vol. 42, no. 23-24, pp. 3453–3459, 1997.

[15] T. Takenaka, H. Habazaki, and H. Konno, "Formation of black anodic films on aluminum in acid electrolytes containing titanium complex anion," *Surface and Coatings Technology*, vol. 169-170, pp. 155–159, 2003.

[16] A. Da Forno, M. Bestetti, N. Lecis, S. P. Trasatti, and M. Trueba, "Anodic oxidation and silane treatment for corrosion protection of AM60B magnesium alloy," *Materials Science Forum*, vol. 690, pp. 413–416, 2011.

[17] F. Zucchi, V. Grassi, A. Frignani, C. Monticelli, and G. Trabanelli, "Influence of a silane treatment on the corrosion resistance of a WE43 magnesium alloy," *Surface and Coatings Technology*, vol. 200, no. 12-13, pp. 4136–4143, 2006.

[18] K. Watanabe, M. Sakairi, H. Takahashi, K. Takahiro, S. Nagata, and S. Hirai, "Anodizing of aluminum coated with silicon oxide by a sol-gel method," *Journal of the Electrochemical Society*, vol. 148, no. 11, pp. B473–B481, 2001.

[19] X. Du and Y. Xu, "Formation of Al_2O_3-$BaTiO_3$ nanocomposite oxide films on etched aluminum foil by sol-gel coating and anodizing," *Journal of Sol-Gel Science and Technology*, vol. 45, no. 1, pp. 57–61, 2008.

[20] J. G. Kaufman, *Properties of Aluminum Alloy*, ASM International, Materials Park, Ohio, USA, 2008.

[21] D. Wang and G. P. Bierwagen, "Sol-gel coatings on metals for corrosion protection," *Progress in Organic Coatings*, vol. 64, no. 4, pp. 327–338, 2009.

[22] M. L. Zheludkevich, J. Tedim, and M. G. S. Ferreira, "'Smart' coatings for active corrosion protection based on multi-functional micro and nanocontainers," *Electrochimica Acta*, vol. 82, pp. 314–323, 2012.

[23] B. R. W. Hinton, "Corrosion inhibition with rare earth metal salts," *Journal of Alloys and Compounds*, vol. 180, no. 1-2, pp. 15–25, 1992.

[24] E. A. Matter, S. Kozhukharov, M. Machkova, and V. Kozhukharov, "Comparison between the inhibition efficiencies of Ce(III) and Ce(IV) ammonium nitrates against corrosion of AA2024 aluminum alloy in solutions of low chloride concentration," *Corrosion Science*, vol. 62, pp. 22–33, 2012.

[25] C. A. Schiller and W. Strunz, "The evaluation of experimental dielectric data of barrier coatings by means of different models," *Electrochimica Acta*, vol. 46, no. 24-25, pp. 3619–3625, 2001.

[26] W. H. Mulder, J. H. Sluyters, T. Pajkossy, and L. Nyikos, "Tafel current at fractal electrodes: connection with admittance spectra," *Journal of Electroanalytical Chemistry*, vol. 285, no. 1-2, pp. 103–115, 1990.

[27] C.-H. Kim, S.-I. Pyun, and J.-H. Kim, "An investigation of the capacitance dispersion on the fractal carbon electrode with edge and basal orientations," *Electrochimica Acta*, vol. 48, no. 23, pp. 3455–3463, 2003.